The Underwater Blast Resistance of Metallic Sandwich Beams With Prismatic Lattice Cores

G. J. McShane
V. S. Deshpande
N. A. Fleck[1]

Department of Engineering,
University of Cambridge,
Trumpington Street,
Cambridge, CB2 1PZ, UK

The finite element method is used to evaluate the underwater blast resistance of monolithic beams and sandwich beams containing prismatic lattice cores (Y-frame and corrugated core) and an ideal foam core. Calculations are performed on both free-standing and end-clamped beams, and fluid-structure interaction effects are accounted for. It is found that the degree of core compression in the free-standing sandwich beam is sensitive to core strength, yet the transmitted impulse is only mildly sensitive to the type of sandwich core. Clamped sandwich beams significantly outperform clamped monolithic beams of equal mass, particularly for stubby beams. The Fleck and Deshpande analytical model for the blast response of sandwich beams is critically assessed by determining the significance of cross-coupling between the three stages of response: in stage I the front face is accelerated by the fluid up to the point of first cavitation, stage II involves compression of the core until the front and back faces have an equal velocity, and in stage III the sandwich beam arrests by a combination of beam bending and stretching. The sensitivity of the response to the relative magnitude of these time scales is assessed by appropriately chosen numerical simulations. Coupling between stages I and II increases the level of transmitted impulse by the fluid by 20–30% for a wide range of core strengths, for both the free-standing and clamped beams. Consequently, the back face deflection of the clamped sandwich beam exceeds that of the fully decoupled model. For stubby beams with a Y-frame and corrugated core, strong coupling exists between the core compression phase (stage II) and the beam bending/stretching phase (stage III); this coupling is beneficial as it results in a reduced deflection of the back (distal) face. In contrast, the phases of core compression (stage II) and beam bending/stretching (stage III) are decoupled for slender beams. The significance of the relative time scales for the three stages of response of the clamped beams are summarized on a performance map that takes as axes the ratios of the time scales. [DOI: 10.1115/1.2198549]

1 Introduction

The underwater blast resistance of sandwich beams remains an active research subject of obvious practical importance to the marine industry. The prototypical problem is sketched in Fig. 1, where a planar underwater blast wave impinges the entire sandwich beam. This is representative of the loading on the outermost structure of a ship by a remote explosion. A number of low strength prismatic sandwich cores have been proposed for application in blast resistant sandwich beams, including the Y-frame of Schelde Shipbuilding[2], the corrugated core and the I-core[3]. The overall aim of this study (and that of the recent investigations reviewed below) is to develop sandwich beams whose blast resistance exceeds that of monolithic beams of equal mass.

Fleck and Deshpande [1] and Xue and Hutchinson [2] have used analytical methods and three-dimensional (3D) finite element (FE) simulations, respectively, to demonstrate that sandwich beams have superior shock resistance to monolithic beams. Fleck and Deshpande [1] developed an analytical model for the shock resistance of clamped sandwich beams by separating the response of these beams into three sequential stages comprising the fluid-structure interaction stage I up to the point of first cavitation, the core compression stage II and finally a combined beam bending and stretching stage III. Both studies decoupled the fluid-structure interaction phase from the structural response and employed the Taylor [3] analysis for a free-standing front face-sheet of the sandwich beam to estimate the momentum transmitted into the beam from the underwater blast wave. A detailed examination of the coupling between the fluid-structure interaction and core compression phases by Deshpande and Fleck [4] demonstrated that the Taylor analysis based upon a free-standing front face-sheet typically underestimates the transmitted momentum for sandwich beams comprising cores with high compressive strengths. This additional fluid-structure interaction was used to explain the difference in predictions between the fully-coupled finite element fluid-structure interaction simulations of Rabczuk et al. [5] and the Fleck and Deshpande [1] analytical model.

Deshpande and Fleck [4] tentatively suggested that low strength sandwich cores endow sandwich beams with enhanced underwater blast resistance: they argue that the low strength core causes sandwich action to begin during the core compression phase, and consequently the back face deflection is reduced. This hypothesis could not be confirmed from the free-standing sandwich beam calculations of Deshpande and Fleck [4]: fully coupled fluid-structure interaction simulations of clamped sandwich beams are required in order to investigate this coupling. In a parallel study, Liang et al. [6] investigated the blast resistance of the sandwich beams with a corrugated core and I-core via fully coupled FE fluid-structure interaction simulations. Their calculations also suggest that weak cores can enhance the blast resistance of sandwich beams. However, the reasons for this enhanced performance are

[1]Author to whom correspondence should be addressed.
[2]Royal Schelde, P.O. Box 16 4380 AA Vlissingen, The Netherlands.
[3]Jos. L. Meyer GmbH, I-Core panels, Industriegebiet Süd, D-26871 Papenburg, Germany.

Contributed by the Applied Mechanics Division of ASME for publication in the JOURNAL OF APPLIED MECHANICS. Manuscript received October 20, 2005; final manuscript received February 16, 2006. Review conducted by R. M. McMeeking. Discussion on the paper should be addressed to the Editor, Prof. Robert M. McMeeking, Journal of Applied Mechanics, Department of Mechanical and Environmental Engineering, University of California – Santa Barbara, Santa Barbara, CA 93106-5070, and will be accepted until four months after final publication of the paper itself in the ASME JOURNAL OF APPLIED MECHANICS.

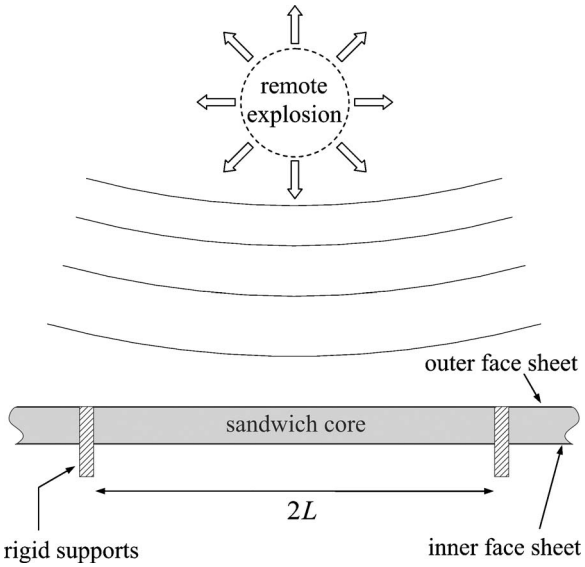

Fig. 1 Schematic of the underwater blast loading of a clamped sandwich beam

unclear from the Liang et al. [6] investigation as the fully coupled simulations are difficult to interpret. In the current study, a set of numerical calculations are reported that switch on and off the coupling between the three stages of response; thereby, the reasons for enhanced performance are determined unambiguously.

Scope of Study

The main aims of this study are:

(i) To compare the underwater blast resistance of sandwich beams with a prismatic Y-frame core, a corrugated core and a foam core of "ideal" strength as defined by Fleck and Deshpande [1], and detailed below.
(ii) To contrast the blast resistance of these sandwich beams with monolithic beams of equal mass.
(iii) To develop an understanding of the effect of cross-coupling between the stages of response in beams with prismatic cores and an ideal foam core. To elucidate this, simulations are performed on both free-standing and end-clamped beams.

The three sandwich cores were chosen in order to span the expected response of a wide range of lattice materials. The Y-frame has a much lower transverse static strength than the corrugated core and ideal foam core, while its longitudinal axial strength and longitudinal shear strength are comparable to those of the other cores. Here the ideal strength foam core with a well-defined isotropic core strength is used solely as a means to clarify the effect of core strength on the sandwich beam response. It gives a useful reference solution by which various topologies can be compared. The ideal strength foam might be representative of stacked cores such as the diamond core [7], and the square honeycomb core [8], but direct comparisons are beyond the scope of the current investigation.

The outline of this paper is as follows. First, the geometries of the sandwich beams are defined. The underwater blast resistance of *free-standing* monolithic and sandwich beams is investigated to determine the transmitted momentum, degree of core compression and the duration of the core compression phase. The use of free-standing beams gives unambiguous results for stages I and II. Next, the fully coupled fluid structure interaction response of *clamped* monolithic and sandwich beams is described. These calculations include stage III. The results for the clamped beams are then contrasted with three sets of decoupled simulations in which we systematically decouple one or more stages of the beam response. Finally, a blast mechanism map is constructed with axes comprising the ratios of the durations of the various phases of beam response.

2 Conceptual Framework

We shall make extensive use of the Fleck-Deshpande [1] framework in order to devise numerical calculations for the sandwich beam response, including a study on the role of overlapping time scales from stage to stage.

Stage I - The Initial Fluid-Structure Interaction Phase. Taylor [3] obtained the solution for a one-dimensional wave in an acoustic fluid impinging a free-standing plate. He demonstrated that fluid cavitation limits the momentum conveyed to the plate; when the plate is light, cavitation occurs early and only a small proportion of the free-wave impulse is transmitted to the plate. Fleck and Deshpande [1] and Xue and Hutchinson [2] followed this approach and similarly computed the momentum transmitted to the sandwich beam by treating the front face of the sandwich beam as a free-standing plate. We briefly review the relevant equations as we shall make use of them below. Consider a representative fluid particle engulfed by a pressure wave traveling at a velocity c_w. The pressure p on the particle of the fluid, of density ρ_w, rises from zero at time $t<0$ to the transient value

$$p = p_0 e^{-t/\theta} \tag{1}$$

for $t \geqslant 0$. Here, p_0 is the peak pressure and θ is the decay constant of the wave. (The values of (p_0, θ) depend upon the details of the underwater explosion.) When this pressure wave hits a stationary rigid plate at normal incidence it imparts an impulse

$$I_0 = 2\int_0^\infty p_0 e^{-t/\theta} dt = 2p_0\theta, \tag{2}$$

to the plate. The factor of 2 arises in (2) due to full reflection of the wave.

If instead, the pressure wave impacts a free-standing plate, the imparted impulse is less than I_0 and can be estimated as follows. When the pressure wave strikes a free-standing plate of thickness h made from a material of density ρ_f, it sets the plate in motion and is partly reflected. The reflected wave causes the pressure in the fluid to drop to zero, and thereby trigger cavitation. This occurs first at the interface between the plate and the fluid after a time

$$\frac{T_1}{\theta} = \frac{1}{\psi - 1} \ln \psi \tag{3}$$

where $\psi \equiv \rho_w c_w \theta/(\rho_f h)$. The momentum per unit area I_t transmitted to the structure is

$$I_t = \zeta I_0, \tag{4a}$$

where

$$\zeta \equiv \psi^{\psi/(1-\psi)} \tag{4b}$$

Fleck and Deshpande [1] assumed that this transmitted impulse imparts a uniform velocity

$$v_0 = I_t/(\rho_f h) \tag{5}$$

to the outer face of the sandwich plate. Now assume some representative values. The sandwich beam has steel faces of density $\rho_f = 7850\ \text{kgm}^{-3}$ and is of thickness $h = 10$ mm. The fluid medium is water of density $\rho_w = 1000\ \text{kgm}^{-3}$ and wave speed $c_w = 1400\ \text{m s}^{-1}$. The primary wave is assumed to possess a decay time $\theta = 0.1$ ms. Then, the fluid-structure interaction parameter has the value $\psi = 1.8$, resulting in a transmitted impulse of $I_t = 0.27 I_0$ from Fig. 4, and a duration of loading $T_1 \approx 0.74\theta = 0.07$ ms via (3).

Stage II–Core Compression Phase. At the start of this phase, the front face has a velocity v_0, while the core and back face are stationary. The finite compressive strength of the core causes the front face to be decelerated and the back face to be accelerated. The final common velocity of the faces and core is dictated by momentum conservation. Fleck and Deshpande [1] derived simple approximate expressions for the degree of core compression and the duration of this phase[4]. They argued that the duration of the core compression phase is

$$T_2 \approx \frac{I_t}{2\sigma_c} \tag{6}$$

where σ_c is the transverse compressive strength of the core. Now substitute some typical values. Upon taking $p_0=100$ MPa for an intense shock, and σ_c in the range 0.5 to 15 MPa, we estimate T_2 to lie in the range 0.1 to 5 ms.

Stage III–Beam Bending and Stretching Phase. At the end of stage II, the sandwich beam has a uniform velocity except for a boundary layer near the supports. The remaining problem to be solved is the classical problem of the impulsive response of a monolithic beam, and Fleck and Deshpande [1] presented an analytical solution by extending the Symmonds [9] analysis to finite deflections. The beam is brought to rest by plastic bending and stretching at a time T_3 given by

$$T_3 \approx L\sqrt{\frac{\rho_{\text{hom}}}{\sigma_{\text{hom}}}} \tag{7}$$

where L is the half-span of the beam and ρ_{hom} and σ_{hom} are the homogenized values of density and longitudinal strength of the beam, respectively. Now consider representative values for the material and geometric parameters. The average axial strength over the cross section of a sandwich beam is of order 60 MPa, and ρ_{hom} is of order 2000 kgm^{-3}. Consequently, T_3 ranges from 5 to 25 ms for beams of half-span 1 to 5 m, respectively.

Fleck and Deshpande [1] derived analytical expressions for the underwater blast response of sandwich beams by assuming that $T_1 \ll T_2 \ll T_3$. With the above choice of physical properties, the three time scales decouple for a slender beam with a strong core. In contrast, the three time scales overlap for a stubby beam with a weak core. We shall investigate the significance of overlapping time scales in some detail below.

2.1 An Hypothesis for the Effect of the Cross-Coupling Between the Stages of Response. It is now argued that the cross-coupling of the three stages of response can be parametrized in terms of the nondimensional groups T_1/T_2 and T_2/T_3 for a sandwich beam. The parameter T_1/T_2 gives a measure of fluid-structure interaction during core compression, while the parameter T_2/T_3 gives a measure of the degree to which beam bending/stretching occurs simultaneously with core compression. Deshpande and Fleck [4] have already investigated the sensitivity of the blast resistance of a free-standing sandwich beam with a foam core to the parameter T_1/T_2. Upon noting that T_1/T_2 is approximately equal to σ_c/p_0 via (3) and (6), we can reinterpret their results for the dependence of transmitted impulse and degree of core crush upon σ_c/p_0. In brief, they noted that the transmitted impulse is almost insensitive to σ_c/p_0 provided this ratio is less than 0.1, while the core compressive strain acquired in stage II is sensitive to σ_c/p_0 over the full range[5]. We conclude that the degree of core crush is much more sensitive to the ratio T_1/T_2 than the level of transmitted impulse.

Define $\bar{w}_p$ as the peak value over the time history of the mid-span back-face deflection, normalized by the corresponding value from a fully decoupled analysis, such as the analytical model of Fleck and Deshpande [1]. In broad terms, we can consider four regimes of behavior for $\bar{w}_p$, depending upon the values of T_1/T_2 and T_2/T_3. These four regimes are summarized in Fig. 2 in the form of a blast mechanism map for the underwater blast response of sandwich beams. The regimes are:

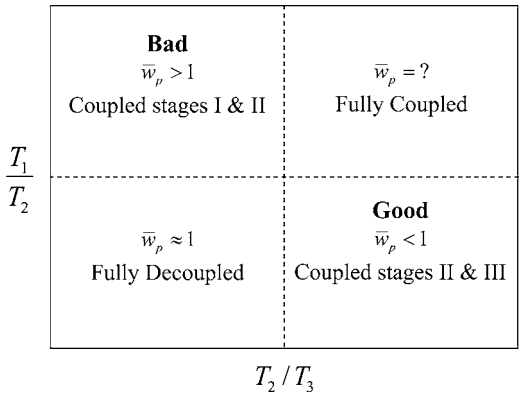

Fig. 2 Schematic of the deformation mechanism map for the underwater blast loading of a sandwich beam. Four regimes of behavior are expected depending on the ratios of the durations of the stages: T_1/T_2 and T_2/T_3. The anticipated values of $\bar{w}_p$ (peak deflection of the beams normalized by the prediction of the decoupled analysis) are included in the sketch.

(i) Low T_1/T_2 and low T_2/T_3, giving $\bar{w}_p \approx 1$. This corresponds to a fully decoupled response from one stage to the next, in the manner assumed by Fleck and Deshpande [1].

(ii) High T_1/T_2 and low T_2/T_3, giving $\bar{w}_p > 1$. Coupling exists between the fluid-structure interaction stage I and the core compression stage II, while the beam bending/stretching phase (stage III) is decoupled. This scenario has already been considered by Deshpande and Fleck [4] for the case of a foam core. They demonstrated that the momentum transmitted into the beam exceeds that predicted by the Taylor analysis (4) based upon a free-standing front face-sheet. In this regime, we expect the beams to undergo larger deflections than that predicted by a decoupled analysis.

(iii) Low T_1/T_2 and high T_2/T_3, giving $\bar{w}_p < 1$. The fluid-structure interaction stage is decoupled from the core compression phase, but the core compression and beam bending and stretching phases are coupled. The response resembles the one-dimensional buffer plate/crushable core as analyzed by Ashby et al. [10]. The front face arrests with little deflection of the back face, and sandwich action (that is, cooperative bending deformation of the faces) does not arise. Consequently, a decoupled analysis is expected to overpredict the back face deflection in this regime.

(iv) High T_1/T_2 and high T_2/T_3. Full coupling exists between all stages and it is difficult to make simplifying approximations. Additional 3D calculations are needed to determine the value of $\bar{w}_p$ in this regime, but this is beyond the scope of this study.

We conclude from the above discussion that the preferred small value of $\bar{w}_p$ is achieved by arranging for a small T_1/T_2 and a high T_2/T_3.

[4]More accurate calculations are reported by Radford et al. [12] but these involve numerical quadratures rather than explicit formulae.

[5]The interested reader is referred to Figs. 14(*a*) and 14(*b*) of Deshpande and Fleck [4].

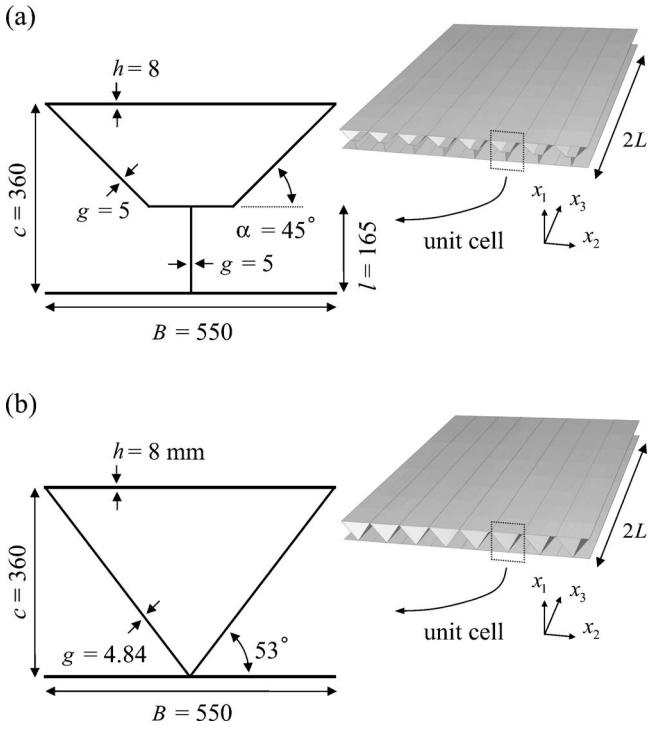

Fig. 3 Sketches of the (*a*) Y-frame (*b*) corrugated core sandwich beams, comprising a large number of repeating units. The prismatic axes of these cores are along the length of the beams. The cross-sectional beam dimensions employed in the FE calculations for the shell reference planes are given in the figure. All dimensions are in millimeters.

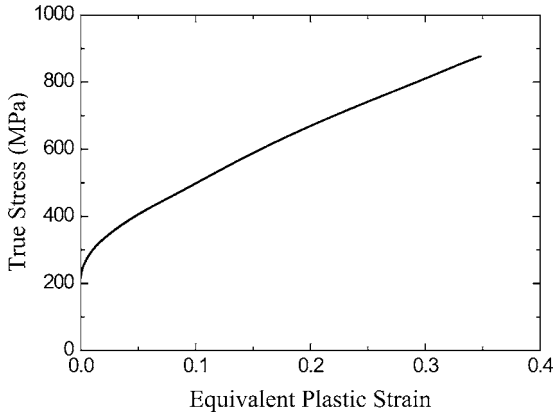

Fig. 4 The uniaxial tensile stress versus strain response of 304 stainless steel as measured by Côté et al. [7,8] and employed in all the calculations reported here

3 Geometry and Material Properties of Sandwich and Monolithic Beams

All beams of span $2L$ are assumed to be made from steel (density of steel $\rho_f = 8000\ \text{kgm}^{-3}$) with a fixed mass per unit area $m_{\text{tot}} = 192\ \text{kgm}^{-2}$, corresponding to a monolithic beam of thickness $d = 24$ mm. The sandwich beams comprise identical front and back face-sheets of thickness $h = 8$ mm and a core of depth $c = 360$ mm. The relative density of the core is $\bar{\rho} = 0.022$. Thus, the only difference between the three types of sandwich beams is the core topology.

The sandwich beams comprise a large number of repeating units, see, for example, the sketches of the Y-frame and corrugated core beams in Figs. 3(*a*) and 3(*b*), respectively. A single unit cell suffices to describe the Y-frame and corrugated core topologies:

(a) The *Y-frame* is sketched in Fig. 3(*a*). It comprises a Y-shaped frame with the prismatic x_3 axis along the beam length. The cross section of the Y-frame is described by the height l of the Y-frame leg, the inclination α of the Y-angles, the thickness g of all the constituent members, the overall core thickness c and the width B of the unit cell. In this study we restrict attention to the Y-frame design as employed by Royal Schelde (the dimensions are detailed in Fig. 3(*a*)).

(b) The *corrugated core* is chosen to ensure a fair comparison between the Y-frame and corrugated core sandwich beams. Both sets of beams have the same overall dimensions, face-sheet thickness, and overall mass. This dictates the sheet thickness of the corrugations to be $g = 4.84$ mm, with a corrugation angle of 53 deg, as sketched in Fig. 3(*b*).

(c) The *ideal foam core*, described as follows. The Y-frame and corrugated cores described above have a relative density (ratio of mass of smeared-out core to the mass of the solid material from which the core is made) of $\bar{\rho} = 0.022$. As a reference case, we also analyze the blast response of a sandwich beam with an "ideal" strength foam core of relative density $\bar{\rho} = 0.022$. As introduced by Fleck and Deshpande [1], this foam core has an isotropic response with a compressive strength $\sigma_c = \bar{\rho}\sigma_Y$, where σ_Y is the yield strength of the solid from which the foam is made and a nominal densification strain $1 - \bar{\rho}$. This is the Voigt upper bound on the strength of the cellular material of relative density $\bar{\rho}$ made from a solid material with yield strength σ_Y. The constitutive response of the foam core is detailed in Sec. 3.1.

In addition to these sandwich beams, a reference *monolithic* steel beam of thickness $d = 24.0$ mm (mass per unit area equal to that of the sandwich beams) is also considered. For each beam geometry, we assume two beam spans: $L = 1$ m and $L = 3$ m.

3.1 Material Properties. The sandwich beams (face-sheets and core) are made from 304 stainless steel of density $\rho_f = 8000\ \text{kgm}^{-3}$. The stainless steel is modeled as a rate independent J2 flow theory solid with Young's modulus $E_s = 210$ GPa, and Poisson's ratio $\nu = 0.3$. The uniaxial tensile true stress versus equivalent plastic strain response of 304 stainless steel has been measured by Côté et al. [7,8] at an applied strain rate of $10^{-3}\ \text{s}^{-1}$, and the measured response is plotted in Fig. 4. This uniaxial tensile curve was assumed in all calculations presented here. Although the actual curve was used, it is clear from Fig. 4 that the material behaves in a bilinear manner, with a Young's modulus of 210 GPa, a yield strength of $\sigma_Y = 217$ MPa and a post-yield linear hardening modulus of $E_t = 2.1$ GPa.

The ideal strength foam core was modeled as a compressible continuum using the metal foam constitutive model of Deshpande and Fleck [11]. Write s_{ij} as the usual deviatoric stress and the von Mises effective stress as $\sigma_e \equiv \sqrt{3 s_{ij} s_{ij}/2}$. The isotropic yield surface for the metal foam is then specified by

$$\hat{\sigma} - Y = 0, \tag{8}$$

where the equivalent stress $\hat{\sigma}$ is a homogeneous function of σ_e and mean stress $\sigma_m \equiv \sigma_{kk}/3$ according to

$$\hat{\sigma}^2 \equiv \frac{1}{1 + (\alpha/3)^2}\left[\sigma_e^2 + \alpha^2 \sigma_m^2\right] \tag{9}$$

The material parameter α denotes the ratio of deviatoric strength to hydrostatic strength, and the normalization factor on the right hand side of relation (9) is chosen such that $\hat{\sigma}$ denotes the stress in

a uniaxial tension or compression test. An over-stress model is employed with the yield stress Y specified by

$$Y = \eta\dot{\hat{\epsilon}}^p + \sigma_c \tag{10}$$

in terms of the viscosity η and the plastic strain-rate $\dot{\hat{\epsilon}}^p$ (work conjugate to $\hat{\sigma}$). The characteristic $\sigma_c(\hat{\epsilon}^p)$ is the static uniaxial stress versus plastic strain relation. Normality of plastic flow is assumed, and this implies that the "plastic Poisson's ratio" $\nu_p = -\dot{\epsilon}^p_{22}/\dot{\epsilon}^p_{11}$ for uniaxial compression in the 1-direction is given by

$$\nu_p = \frac{1/2 - (\alpha/3)^2}{1 + (\alpha/3)^2} \tag{11}$$

In the simulations, the ideal strength foam is assumed to have a Young's modulus $E_c = \bar{\rho}E_s$, an elastic Poisson's ratio $\nu = 0.3$, and a plastic Poisson's ratio $\nu_p = 0$ [10]. The static strength σ_c versus equivalent plastic strain $\hat{\epsilon}^p$ history is taken as

$$\sigma_c = \begin{cases} \bar{\rho}\sigma_Y, & \hat{\epsilon}^p \leqslant \epsilon_D \\ \bar{\rho}\sigma_Y + E_f(\hat{\epsilon}^p - \epsilon_D), & \text{otherwise} \end{cases} \tag{12}$$

where $\epsilon_D \equiv -\ln(\bar{\rho})$ is the logarithmic densification strain beyond which negligible plastic straining of the foam occurs. The viscosity η in the foam core was set to 0.86×10^{-3} MPa s. This ensures that the shock width is approximately $c/10$ for the range of the calculations reported here; see Radford et al. [12] for details of the shock width calculation.

4 Finite Element Calculations

The explicit time integration version of the commercial finite element package ABAQUS was used to calculate the underwater blast response of (i) a free-standing sandwich beam (Fig. 5(*a*)) and (ii) a clamped sandwich beam (Fig. 5(*b*)). Two-dimensional analyses sufficed to investigate the underwater blast response of the free-standing beams. The clamped beam simulations required three-dimensional analyses for the Y-frame and corrugated core beams while two-dimensional plane strain analyses sufficed for the clamped sandwich beams with an ideal strength foam core. Perfect bonding between core and face-sheets is assumed in all sandwich beams. The ABAQUS "general contact" option (which includes self-contact) was used to enforce a hard contact between all surfaces for the lattice cores in order to include the effect of core densification.

The monolithic beams were modeled using four-noded plane strain quadrilaterals (CPE4R in the ABAQUS notation). Typically, ten elements were used in the through-thickness direction of the beam and about 200 elements exist along the beam length.

4.1 The Fluid Column. All calculations were performed using the free-field pressure versus time characteristic (1) with $\theta = 0.1$ ms and p_0 in the range 60 to 180 MPa. The fluid was taken to be water, treated here as an acoustic medium with density $\rho_w = 1.0$ Mg m^{-3}, bulk modulus $E_w = 1.96$ GPa, and wave speed $c_w \equiv \sqrt{E_w/\rho_w} = 1400$ m s^{-1}. The fluid is assumed to be unable to sustain tensile loading, which implies that the cavitation pressure is $p_c = 0$ MPa.

The fluid column (in both the free-standing and clamped beam simulations) was modeled using acoustic elements: eight-node bricks in 3D, and four-node quadrilaterals in the plane strain analyses (AC3D8R and AC2D4R, respectively, in ABAQUS notation). The fluid column represents a semi-infinite fluid in order to model a far field explosion. However, refinement of the mesh in the fluid is necessary to ensure minimal numerical dispersion of the blast wave. As discussed by Sprague [13], it is desirable to have a small fluid-column with the pressure history (1) applied as close to the structure as possible. We thus employ a fluid-column of height $H = 1$ m in all calculations and use the following prescription to ensure minimal reflections from the top of the column,

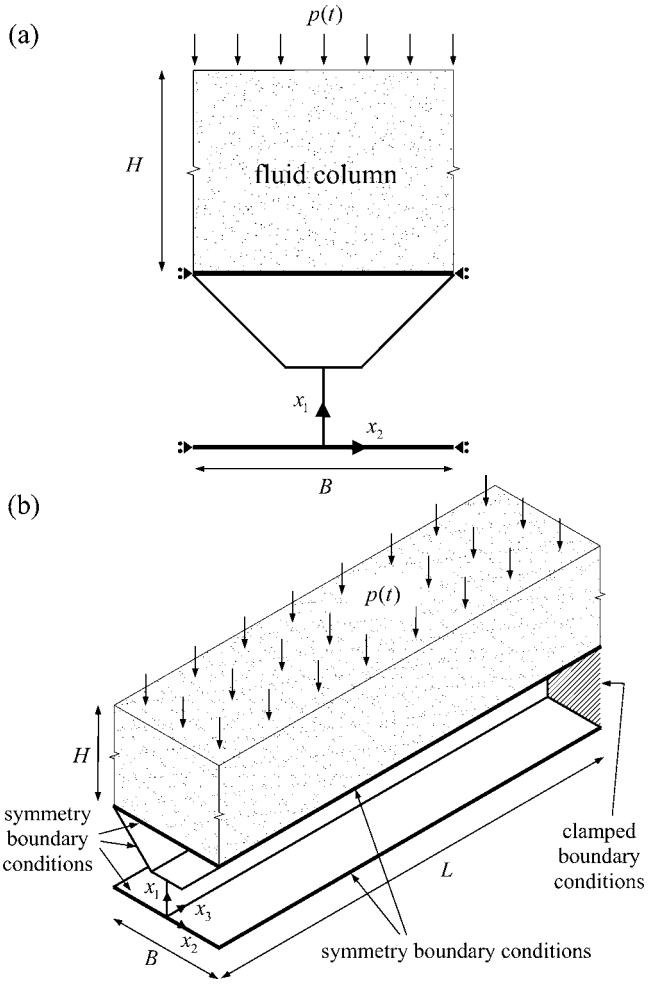

Fig. 5 Boundary value problems analyzed for the underwater blast loading of (*a*) the free-standing and (*b*) the clamped sandwich beam. Only the Y-frame core beams are shown in this figure.

thereby simulating a semi-infinite column.

The fluid column was divided into two equal halves, each of height 0.5 m with a horizontal layer of nodes along the interface. The bottom half in contact with the structure was discretized by elements of height 10 mm and the pressure boundary condition (1) was applied on the surface separating the two halves of the fluid column. The top half of the column was discretized using elements of height 40 mm and an impendence boundary condition

$$\dot{u} = \frac{p}{\rho_w c_w} \tag{13}$$

on the top surface of the column, where $\dot{u}$ is the particle velocity normal to the top surface and p is the fluid pressure. This boundary condition ensures no reflection of the waves from the top surface thereby simulating a semi-infinite column.

The pressure boundary condition (1) was applied to the horizontal layer of nodes separating the two halves of the column, in two steps. Step 1 has duration 0.69 ms and the pressure history (1) is applied throughout this step. The duration of this step is less than the time required for the wave reflected from the structure to reach the horizontal layer of nodes where the pressure boundary condition is specified. In step 2, no pressure was specified on the boundary separating the two halves of the fluid-column. This permits the reflected wave to pass through unimpeded. Note that although we only specify the pressure history (1) for 0.69 ms, 99.9% of the blast impulse is applied in this period since we have

made the choice $\theta=0.1$ ms in all calculations.

This prescription for the fluid column and application of the pressure wave (1) gave excellent agreement between analytically known fluid-structure interaction solutions and the numerical results. For example, the cavitation time and transmitted impulse predicted by the FE simulations were nearly identical to the Taylor [3] prediction for a variety of thicknesses of steel plate.

4.2 Free-Standing Beam Simulations. A sketch of the boundary value problem analyzed to investigate the underwater blast response of free-standing beams is shown in Fig. 5(*a*). In these two-dimensional calculations, the sandwich beam is free to move in the x_1-direction and constrained from motion in the x_2-direction via symmetry boundary conditions. The beams with an ideal foam core were modeled using four-noded quadrilaterals (CPE4R in the ABAQUS notation) in both the faces and core, with about 180 elements in the x_1-direction. The beams with a Y-frame core and a corrugated core were modeled using two-dimensional linear Timoshenko beam elements (B21 in ABAQUS notation) with elements of thickness 8 mm and 10 mm used to discretize each core strut and face-sheet, respectively. The symmetry boundary conditions for the Y-frame core and corrugated core entail zero rotation and zero displacement in the x_2-direction.

4.3 Clamped Beam Simulations. The boundary value problem comprises a clamped beam subjected to a far-field underwater explosion, as sketched in Fig. 5(*b*). Only half of the beam is analyzed and symmetry boundary conditions are specified on the x_1-x_2 plane at midspan ($x_3=0$); the beam (core and face-sheets) is clamped at the other end ($x_3=L$). These fully clamped boundary conditions have been employed in prior investigations (see for example Fleck and Deshpande [1] and Xue and Hutchinson [2]) and are considered appropriate for ship hulls where the bulkhead extends to the outer hull. We note that Liang et al. [6] have employed boundary conditions wherein only the inner face is fixed at the two outer supports. The effect of the choice of boundary conditions on the sandwich beam response is not within the scope of the present investigation, but clearly is important.

The beams with an ideal foam core are again modeled using plane strain elements (approximately 180 and 200 elements in the x_1- and x_3-directions, respectively). The Y-frame and corrugated core beams for the clamped beam analysis were generated in ABAQUS by extruding the respective cross sections (Figs. 3(*a*) and 3(*b*)) to the required lengths. These beams were then discretized using the 3D shell elements (S4R in the ABAQUS notation). Typically, 5500 elements were used to discretize each face-sheet and 11,000 elements were used in the core. In these 3D analyses, symmetry boundary conditions are specified on the x_1-x_3 planes at $x_2=\pm B/2$ in order to represent repeating units of the Y-frame and corrugated core in the x_2-direction (see Fig. 3).

5 Blast Response of Free-Standing Sandwich Beams

We first consider the blast response of free-standing sandwich beams due to an underwater blast wave impinging the front face, as sketched in Fig. 5(*a*). The beams are free to move in the x_1-direction but are constrained from motion in the x_2-direction via symmetry boundary conditions (consistent with the notion that we are analyzing a representative section of a panel comprising a large number of repeating units). Beam bending and stretching (stage III) effects are absent, and we use these calculations to investigate the coupling between stages I and II of the beam response and hence determine the (i) transmitted momentum, (ii) degree of core compression and (iii) times at which stages I and II end.

5.1 Results. The progressive increase in normalized momentum I/I_o of the entire sandwich beam with increasing normalized time t/θ (measured from the instant of the shock wave impinging on the structure) is plotted in Figs. 6(*a*) and 6(*b*) for peak blast pressures $p_o=100$ MPa and 180 MPa, respectively. Each of the

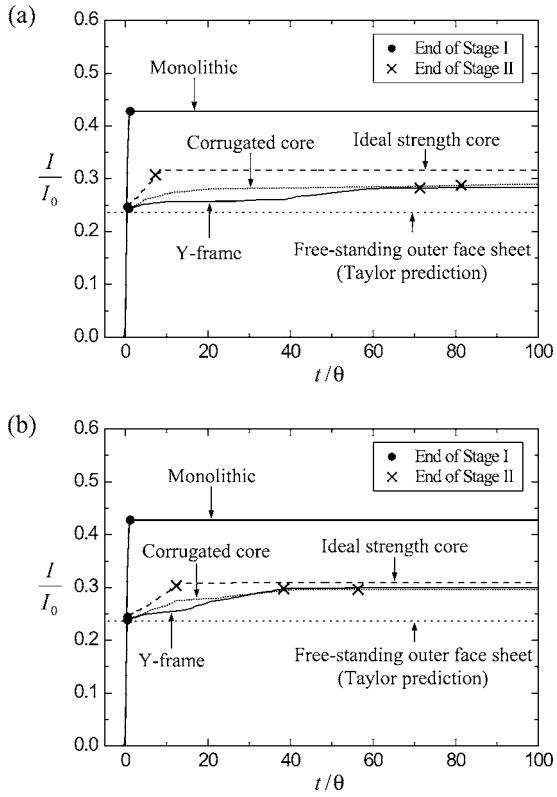

Fig. 6 The time variations of the momenta of the free-standing sandwich and monolithic plates for blast pressures (*a*) $p_0=100$ MPa and (*b*) $p_0=180$ MPa. The Taylor prediction of the final transmitted momentum into the sandwich plate based on a free-standing front face-sheet is also included.

sandwich beams rapidly acquires momentum, followed by a more gradual increase. Finally, the sandwich plate separates from the water and the ensuing momentum remains constant. Stage I of the response ends (by definition at the first cavitation of the water) at $t/\theta\approx 1$ for the monolithic and sandwich beams, while Stage II ends (as defined by the peak core compression being attained) much later at $t/\theta\sim 10-80$ for the various sandwich beams. The end of each stage is marked on the plots of Fig. 6. The beam with an ideal strength core acquires a slightly higher transmitted momentum over a much shorter time than the Y-frame and corrugated core beams. The momentum transmitted into each of the sandwich beams is less than that for a monolithic beam of equal mass but exceeds the Fleck and Deshpande [1] prediction based upon a free-standing front face-sheet.

The through-thickness core compression is related to the average reduction Δc in core thickness by $\epsilon_{fs}(t)\equiv\Delta c/c$, and is plotted in Fig. 7 (the core compression was obtained by averaging the displacements of the front and back faces over the beam width B). For both values of p_0, the Y-frame undergoes the maximum core compression, while the ideal core compresses least. The ends of stages I and II are also in Fig. 7. For each beam, and at both pressure levels, the time to maximum core compression in Fig. 7 defines the duration of stage II and approximates the time for the transmitted momentum to asymptote to the maximum value in Fig. 6. (The end of stage II marked in Fig. 6 corresponds to the time at which this maximum core compression is achieved.)

The effect of the free-field impulse I_0 upon the transmitted impulse I_t/I_0, duration of stage II T_2/θ and degree of core compression $\epsilon_{fs}^{\max}$ are summarized in Fig. 8 for the free-standing beams. These calculations have been performed by varying p_0 with θ held fixed at 0.1 ms. Observe that the normalized transmitted impulse is reasonably independent of the level of blast impulse and is

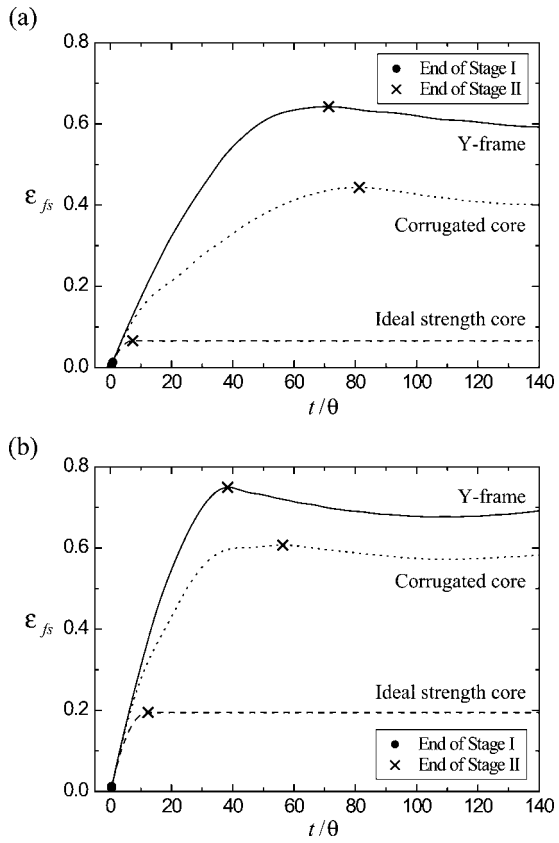

Fig. 7 The time evolution of core compression ε_{fs} in the free-standing sandwich beams for blast pressures (*a*) p_0=100 MPa and (*b*) p_0=180 MPa

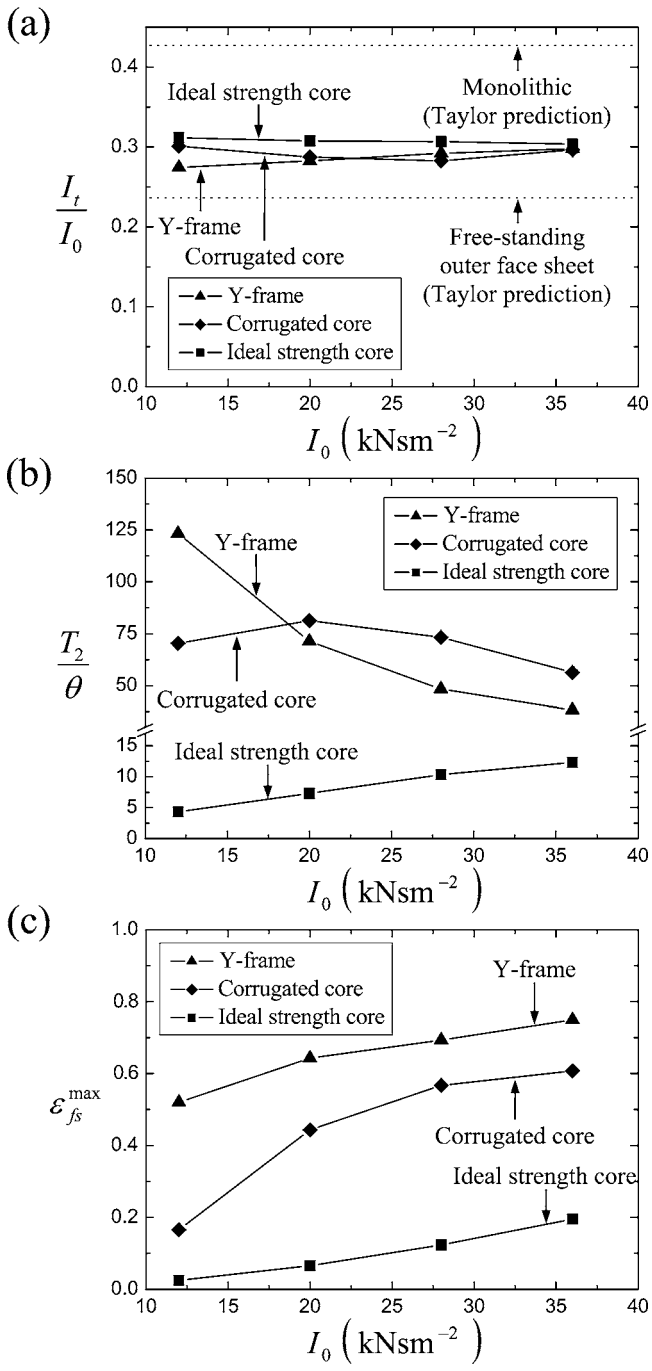

Fig. 8 Finite element predictions of the (*a*) normalized transmitted momentum I_t/I_0, (*b*) normalized duration of core compression T_2/θ and (*c*) peak core compression ε_{fs}^{max} as a function of the blast impulse for free-standing monolithic and sandwich beams

approximately equal for all beams; I_t is intermediate between that predicted for a free-standing front face and that transmitted into a monolithic beam of mass equal to that of the sandwich beam. In contrast, the duration of stage II, T_2, and the core compression strain ϵ_{fs}^{max} are sensitive to the level of applied impulse I_0. Both T_2 and the peak core compression ϵ_{fs}^{max} are much greater for the sandwich beams with corrugated and Y-frame cores than for the sandwich beams with an ideal strength foam core.

Recall that the Taylor analysis predicts a fluid-structure interaction period up to first cavitation in stage I of duration about θ. The present free-standing beam calculations reveal that an additional 20–30% momentum is transmitted during the stage II period of core compression. After first cavitation, the fluid continues to load the structure. The duration of stage II is 5θ–80θ for the corrugated and Y-frame sandwich beams and 5θ–10θ for the ideal strength foam core. Since the duration of stage III scales with the length L of the beam by (7), we anticipate that time-decoupling of stages II and III may not hold for short span corrugated and Y-frame sandwich beams. The significance of this temporal overlap is explored below where we investigate the blast response of clamped sandwich beams.

6 Blast Response of Clamped Sandwich Beams

Consider the underwater blast response of clamped sandwich beams with geometry and material properties described in Sec. 3. The boundary value problem under consideration is sketched in Fig. 5(*b*). A one-dimensional blast wave as defined by (1) loads a clamped sandwich beam. Both the core and the face-sheets of the sandwich beam are fully clamped, as in the analyses of Fleck and Deshpande [1] and Xue and Hutchinson [2]. In order to investigate the coupling between stages II and III of the response, we consider two sandwich configurations with L=1 m and 3 m, and all other parameters are held fixed at the reference values detailed in Sec. 3.

6.1 Fully Coupled Calculations for Clamped Sandwich Beams. The normalized transverse midspan deflections w/L of the back face-sheet of the L=1 m sandwich and monolithic beams (p_0=100 MPa) are plotted in Fig. 9(*a*) as a function of the normalized time $\bar{t}=t/(L\sqrt{\rho_f/\sigma_Y})$, where t is measured from the instant of the shock wave impinging the beams. The corresponding transient mid-span core compression $\epsilon_c(\bar{t})$ is given in Fig. 9(*b*) for the

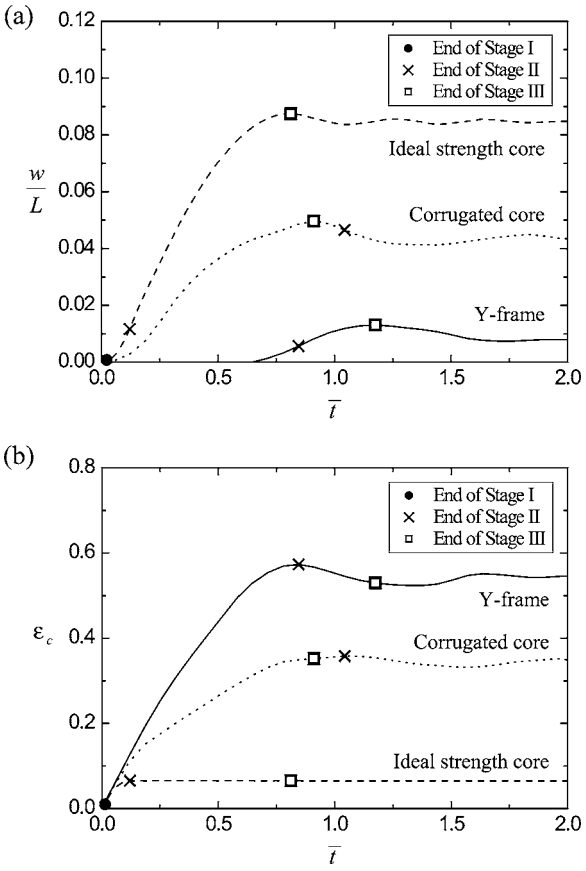

Fig. 9 The time variation of (*a*) normalized deflections of the midspan of the back face *w*/*L* and (*b*) midspan core compression of the *L*=1 m clamped beams subject to a p_0=100 MPa blast. Both the back face deflections and core compressions are obtained by spatially averaging the deflections over the width *B* at the midspans.

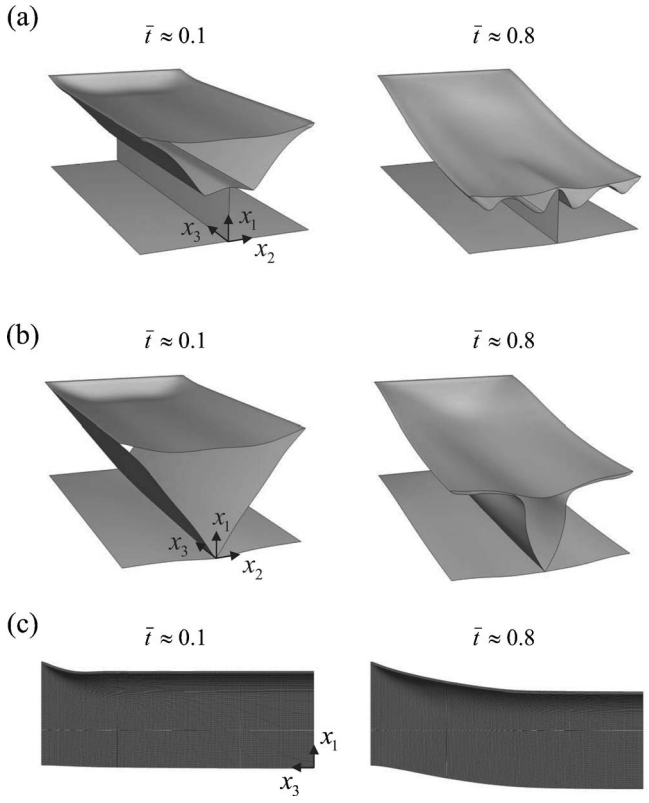

Fig. 10 Finite element predictions of the deformation modes of the *L*=1 m. (*a*) Y-frame, (*b*) corrugated core, and (*c*) ideal strength foam core clamped sandwich beams at $\bar{t}\approx$0.1 and 0.8 for p_0=100 MPa.

three sandwich beams. Both the back face deflections and core compressions were obtained by averaging the midspan deflections over the width *B* of the sandwich beams. Stage I ends early at $\bar{t} \approx 0.02$ for all three types of sandwich beams. For the beam with an ideal foam core, maximum core compression signifies the end of stage II at $\bar{t}\approx 0.1$ while stage III ends at the point of peak back face deflection at $\bar{t}\approx 0.8$. The stage II response of the beams with a Y-frame and a corrugated core is simultaneous with stage III and ends at $\bar{t}\approx 1.0$. Note the reverse ordering of the three cores in Fig. 9(*a*) and 9(*b*): the Y-frame core has the lowest back face deflection, and this is associated with the largest degree of core crush. This is reminiscent of the behavior noted by Liang et al. [6] for stubby beams with a weak core: their assumed boundary conditions were such that the front face behaved as a flyer plate against the weak core, and produced minimal back face deflection.

The FE predictions of the deformation modes (at two selected values of time $\bar{t}$) of the *L*=1 m sandwich beams subjected to a p_0=100 MPa blast are shown in Fig. 10. The core compression of the Y-frame (Fig. 10(*a*)) is accommodated mainly by the deformation of the webs of the Y-frame while the compression of the corrugated core is more uniform (Fig. 10(*b*)). The ideal strength beams undergo smaller core compression (Fig. 10(*c*)), with almost complete densification near the front face-sheet and nearly no deformation adjacent to the back face-sheet due to the propagation and arrest of a plastic shock wave.

The peak midspan back face deflection w_p/L is plotted as a function of blast impulse I_0 in Fig. 11(*a*) for the *L*=1 m monolithic and sandwich beams. Additionally, the core compressive strain $\epsilon_c^{\max}$ (normalized by the corresponding maximum core compressions in the free-standing sandwich beams $\epsilon_{fs}^{\max}$ of Fig. 8(*c*)) is plotted against I_0 in Fig. 11(*b*); and the time T_3 required to achieve peak back face deflection (normalized by the time T_2 required to achieve maximum core compression in the corresponding free-standing sandwich beam calculations of Fig. 8(*b*)) is plotted against I_0 in Fig. 11(*c*). It is evident from Fig. 11(*a*) that the midspan deflection of the sandwich beams is significantly less than that of the monolithic beam of equal mass. With back face deflection taken as the performance metric, the Y-frame and corrugated core beams have a comparable performance and outperform the sandwich beam with an ideal strength core. For the sandwich beams with an the ideal strength core we find that $T_3 \gg T_2$, and so the beam bending/stretching stage III is decoupled from the core compression stage II. This is consistent with the fact that the degree of core compression in the free-standing and clamped beams are similar (see Fig. 11(*b*)). In contrast, the degree of core compression in the clamped Y-frame and corrugated core sandwich beam calculations differs from that in the free-standing sandwich beam calculations (see Fig. 11(*b*)). This is due to the fact that the structural response time T_3 is comparable to the core compression time T_2 for the sandwich beams with a Y-frame core or corrugated core.

The blast response of the *L*=3 m sandwich and monolithic beams is shown in Fig. 12: w_p/L, $\epsilon_c^{\max}/\epsilon_{fs}^{\max}$, and T_3/T_2 are each plotted against I_0 for each beam. Again, the sandwich beams outperform the monolithic beam in the sense that w_p/L is reduced. There is only a minor variation in rear face deflection for the different sandwich beams, in contrast to the case of *L*=1 m shown in Fig. 11(*a*). The structural response time of the *L*=3 m sandwich beams is about three times greater than that of the *L*=1 m beams, as anticipated by relation (7). The ratios T_3/T_2 exceed unity for all

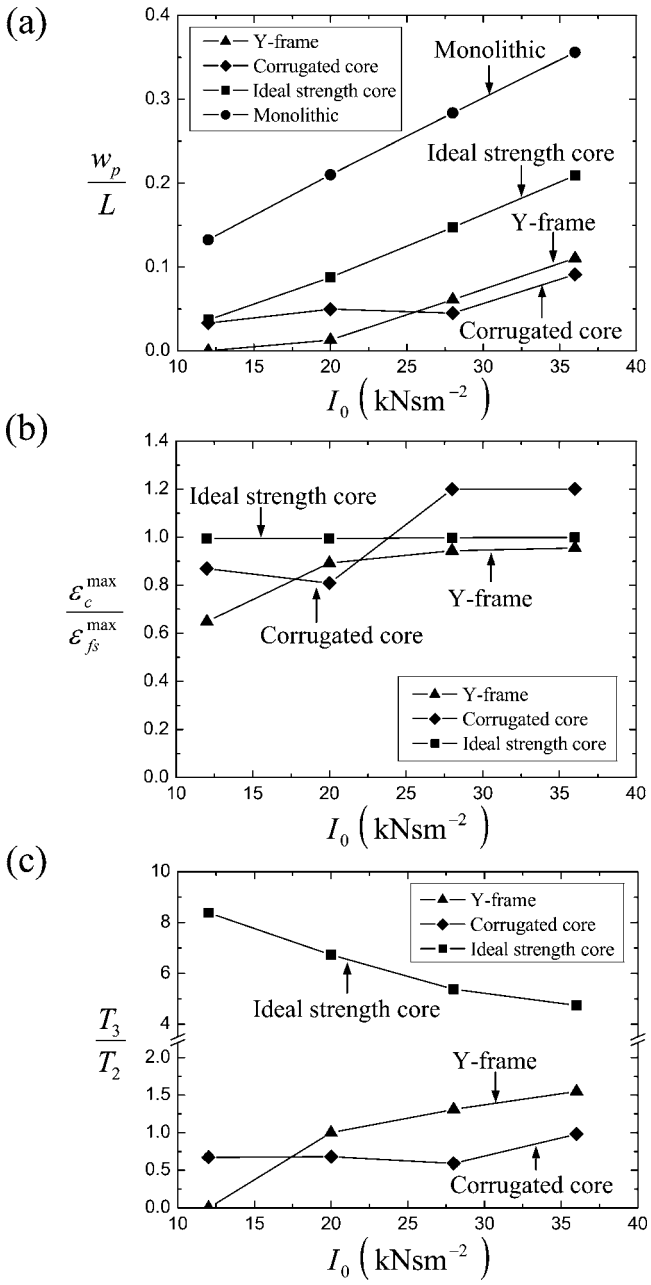

Fig. 11 Finite element predictions of the (*a*) peak normalized back face deflections w_p/L, (*b*) normalized peak core compression $\varepsilon_c^{\max}/\varepsilon_{fs}^{\max}$, and (*c*) normalized time required to attain the maximum deflection T_3/T_2 as a function of blast impulse for the $L=1$ m clamped monolithic and sandwich beams

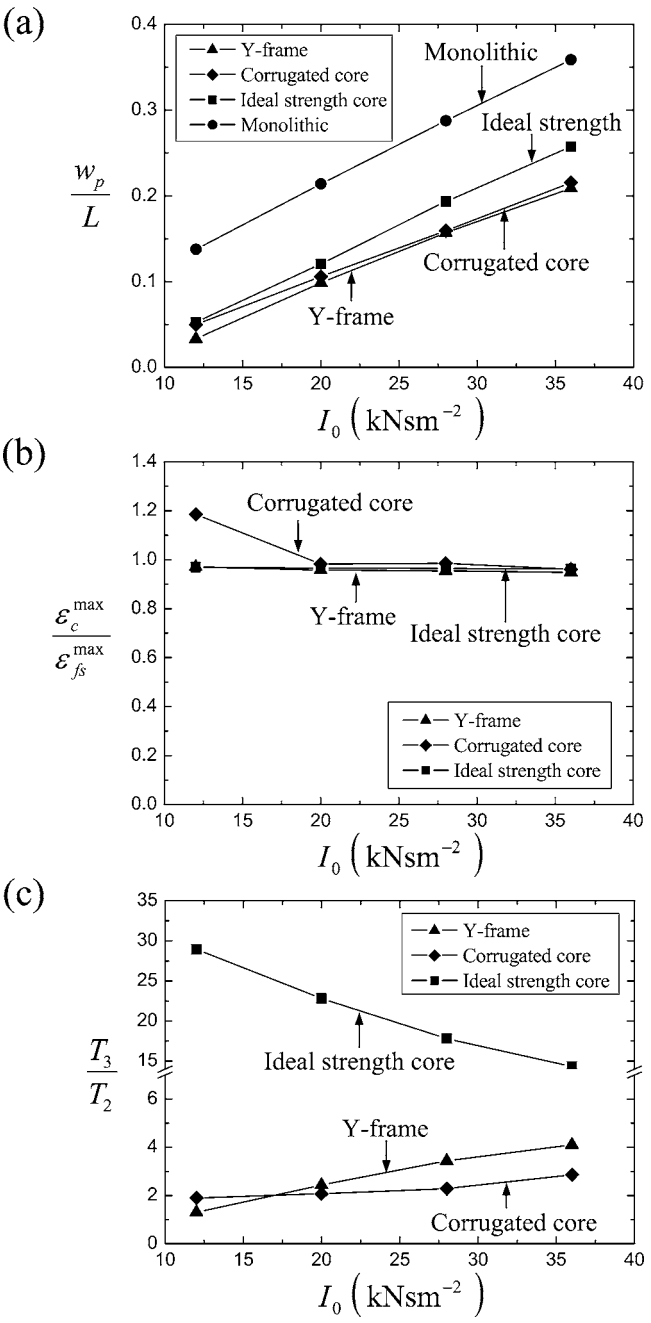

Fig. 12 Finite element predictions of the (*a*) peak normalized back face deflections w_p/L, (*b*) normalized peak core compression $\varepsilon_c^{\max}/\varepsilon_{fs}^{\max}$ and (*c*) normalized time required to attain the maximum deflection T_3/T_2 as a function of blast impulse for the $L=3$ m clamped monolithic and sandwich beams

the sandwich beams (Fig. 12(*c*)), implying that stages II and III are decoupled. Consistently, the core compression predictions from the free-standing and clamped beam simulation are almost identical for all the sandwich cores considered here (refer to Fig. 12(*b*)).

7 An Assessment of the Cross-Coupling Between the Three Stages of Response for the Clamped Sandwich Beam

The superior performance of the Y-frame and corrugated core beams over both the ideal strength foam core sandwich beams and monolithic beams of equal mass is evident from the above calculations for a fully clamped sandwich beam over a wide range of imposed impulses. Here we attempt to explain this performance enhancement within the Fleck and Deshpande [1] conceptual framework. For this purpose we consider the following three sets of calculations for the sandwich beams.

(i) Decoupled Stage I, Denoted by I/II+III. These simulations decouple stage I from the remaining stages by applying an initial uniform velocity to the front face only of the sandwich beam in accordance with the Taylor prediction (5), with no subsequent interaction between the clamped sandwich beam and the fluid. This type of loading was assumed in the previous finite element studies of Xue and Hutchinson [2] and Qiu et al. [14]. A decoupled stage I response is achieved when T_1/T_2 is much less than

unity, or equivalently when σ_c/p_0 is small via (2), (3), and (6). Recall that the full simulations reported above demonstrate that continued fluid loading occurs during stages II and III. Consequently, a comparison of the results for the fully coupled case and for the decoupled stage I case provides an assessment of the significance of fluid-structure interaction in stages II and III. The fully coupled simulations reveal that an additional 20–30% impulse is transmitted during stage II, and thus it is anticipated that the decoupled stage I simulations will result in somewhat smaller back face deflections than the fully coupled case. (For consistency of notation, we shall refer to the fully coupled case by *I+II+III*.)

For the monolithic beams, the only meaningful decoupled calculation is the decoupled stage I calculation, *I/II+III* (or equivalently *I/III* as no core compression exists for monolithic beams), where we impart the velocity (5) to the monolithic beam based upon the Taylor [3] free-standing plate analysis. This corresponds to impulsive loading of the monolithic beam with the impulse given by the Taylor [3] analysis.

(ii) Decoupled Stage III, Denoted by I+II/III. This is achieved by fluid-loading of the free standing beam in stages I and II. At the instant when the faces and core of the sandwich beam share a common velocity, the ends of the sandwich beam are clamped and the beam is allowed to be brought to rest by a combination of plastic bending and stretching in the absence of a fluid. Thus, these simulations switch off any fluid-structure interaction in stage III, and additionally switch off any beneficial coupling between stages II and III. We shall show below that the contribution to the beam displacement is negligible due to pressure loading by the fluid in stage III. However, the cross-coupling between stages II and III significantly reduces the rear face deflection of the clamped sandwich beam for stubby beams with a weak core. We anticipate that the simulations that decouple stage III will produce a greater deflection than the fully coupled case *I+II+III*.

(iii) Fully decoupled, Denoted by I/II/III. The fully decoupled case considers a freely supported beam with its front face given an initial velocity according to the Taylor [3] result (5). The fluid is absent in stages II and III. After the core has finished compressing in stage II, end clamps are applied instantaneously to the beam and the beam is allowed to arrest by bending/stretching in stage III. Now compare this analysis to the fully coupled case *I+II+III*. The fully coupled problem involves 20–30% additional momentum transfer in stage II than that given by the Taylor prediction, but the coupled analysis includes the beneficial coupling between stages II and III, particularly for stubby beams with a weak core. Consequently, it is anticipated that the decoupled numerical analysis will give predictions which are reasonably close to the predictions of the fully coupled analysis. Recall that the analytical model of Fleck and Deshpande [1] also assumes decoupling from one stage to the next.

These decoupled calculations were performed using the finite element meshes described in Sec. 4. The boundary conditions are as specified above (all other boundary conditions being the same as those in the fully coupled simulations). We proceed to present numerical predictions for the maximum midspan back face deflections w_p/L from the above partially and fully decoupled simulations and compare them with the fully coupled predictions. Note that the transverse deflection w is always measured from the clamped supports. The fully coupled finite element calculations reported above for the free-standing and clamped beams have revealed that the deformation mode of the Y-frame resembles that of the corrugated core, while the beams with an ideal foam core display a markedly different behavior. We first explore the significance of cross-coupling between the three stages of response for the Y-frame and corrugated cores and then consider the beams with an ideal foam core.

7.1 The Y-frame and Corrugated Core Beams. Comparisons between the decoupled and fully coupled predictions for the

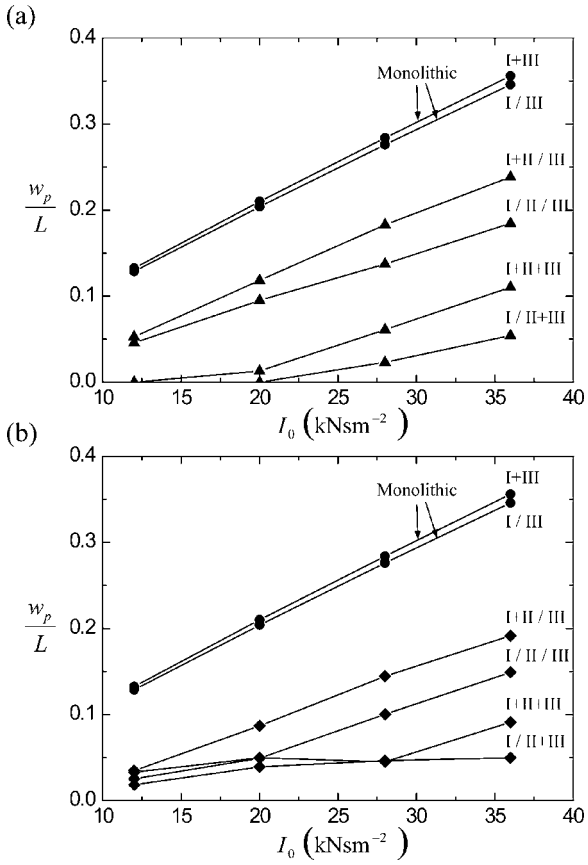

Fig. 13 Comparisons between the fully coupled (*I+II+III*) and decoupled finite element predictions of the peak normalized back face deflections w_p/L of the $L=1$ m (*a*) Y-frame and (*b*) corrugated core clamped sandwich beams. The decoupled calculations for the sandwich beams are the (i) fully decoupled (*I/II/III*), (ii) the decoupled stage I (*I/II+III*), and (iii) the decoupled stage III (*I+II/III*) calculations. The fully coupled and decoupled stage I predictions for the $L=1$ m monolithic beams are included.

$L=1$ m Y-frame and corrugated core beams are shown in Figs. 13(*a*) and 13(*b*), respectively. In general, the fully decoupled analysis *I/II/III* and decoupled stage III analysis *I+II/III* overpredict the maximum midspan deflection w_p while the decoupled stage I analysis underpredicts w_p for the $L=1$ m sandwich beams. On the other hand, the decoupled stage I calculation *I/II+III* for the monolithic beam is in good agreement with the fully coupled predictions *I+II+III*. These results are rationalized as follows.

(a) The decoupled stage I calculation underpredicts the deflection because the Taylor prediction based on a free-standing outer-face-sheet underpredicts the momentum transmitted to the Y-frame and corrugated core beams (see Fig. 8(*a*)).

(b) Peak core compression and back face deflection are attained approximately simultaneously in the $L=1$ m Y-frame and corrugated core beams (Fig. 9). This strong coupling between stages II and III results in reduced back face deflections: the bending action in the sandwich beam occurs at the same time as core crush. Thus, the decoupled stage III calculations overpredict the deflection.

(c) The fully decoupled calculations *I/II/III* only slightly overpredict the deflections as the competing effects (a) and (b) mitigate against each other.

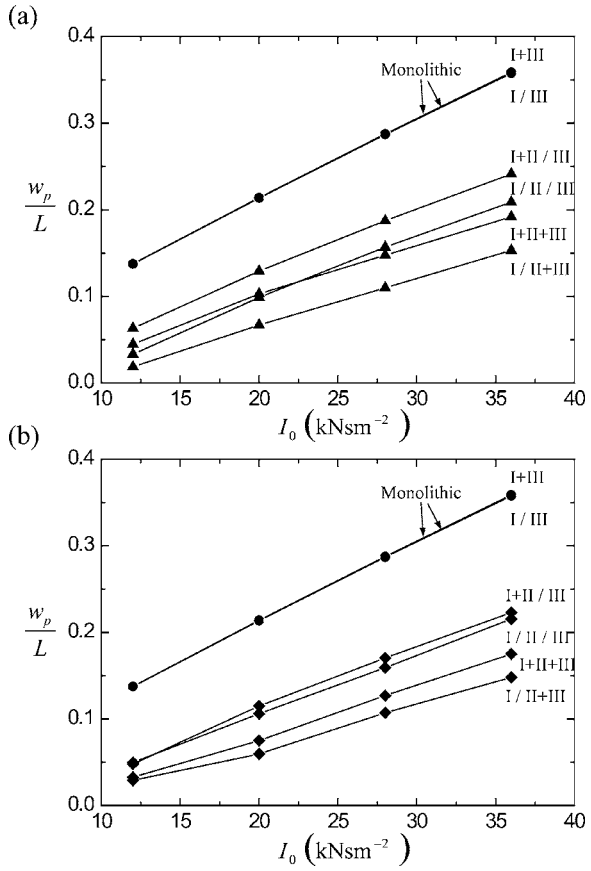

Fig. 14 Comparisons between the fully coupled (*I+II+III*) and decoupled finite element predictions of the peak normalized back face deflections w_p/L of the $L=3$ m (*a*) Y-frame and (*b*) corrugated core clamped sandwich beams. The decoupled calculations for the sandwich beams are the (i) fully decoupled (*I//II//III*), (ii) the decoupled stage I (*I//II+III*), and (iii) the decoupled stage III (*I+II//III*) calculations. The fully coupled and decoupled stage I predictions for the $L=1$ m monolithic beams are included.

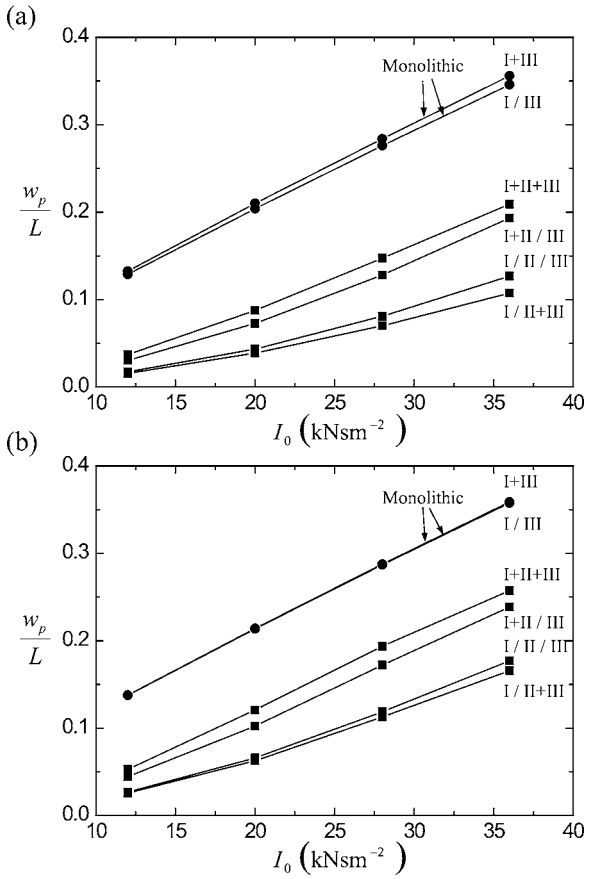

Fig. 15 Comparisons between the fully coupled (*I+II+III*) and decoupled finite element predictions of the peak normalized back face deflections w_p/L of the (*a*) $L=1$ m and (*b*) $L=3$ m ideal strength core clamped sandwich beams. The decoupled calculations for the sandwich beams are the (i) fully decoupled (*I//II//III*), (ii) the decoupled stage I (*I//II+III*), and (iii) the decoupled stage III (*I+II//III*) calculations. The fully coupled and decoupled stage I predictions for the $L=1$ m and $L=3$ m monolithic beams are included.

Similar comparisons between the decoupled and fully coupled predictions of the $L=3$ m Y-frame and corrugated core beams are shown in Figs. 14(*a*) and 14(*b*), respectively. For these slender sandwich beams, there is negligible coupling between stages II and III, and so the decoupled stage III calculations are in good agreement with the fully coupled predictions. On the other hand, the decoupled stage I calculations (and the fully decoupled calculations) underpredict the deflection as the transmitted impulse is underestimated by a Taylor analysis based on the free-standing front face-sheet. Note that the decoupled and fully coupled monolithic beam calculations are in excellent agreement for the $L=3$ m sandwich beams.

7.2 Ideal Strength Core. Comparisons between the various decoupled and fully coupled predictions for the maximum midspan back face deflections of the ideal strength core beams are shown in Figs. 15(*a*) and 15(*b*) for the $L=1$ and 3 m beams, respectively. Unlike the Y-frame and corrugated core beams, the degree of cross-coupling between the three stages of response is similar for the two lengths of sandwich beam. The decoupled stage III calculations slightly underpredict the deflections, while the decoupled stage I and fully decoupled predictions are substantially lower than the fully coupled estimates. These results are understood as follows.

(a) The duration of the beam bending and stretching phases greatly exceeds the duration of the core compression phase in these beams with strong cores (Figs. 11 and 12). Thus, stage III is decoupled from stages I and II and the decoupled stage III calculation only slightly underestimates the fully coupled predictions for both beam lengths.

(b) Similar to the Y-frame and corrugated core beams, the Taylor analysis based on a free-standing front face-sheet underestimates the momentum transmitted into the ideal strength foam core beams (Fig. 8(*a*)). Thus, the decoupled stage I and fully decoupled calculations under-predict the deflection. Since there is negligible coupling between stage III and stages I and II, the fully decoupled calculation and the decoupled stage I calculation predict approximately equal deflections.

7.3 Effect of Transmitted Impulse in Stage III. The transmitted impulse is plotted in Fig. 16 as a function of $\bar{t}$ for the case of a 100 MPa blast wave impinging the clamped sandwich beams (Y-frame, corrugated core and ideal strength foam core) and clamped monolithic beams with half-span $L=1$ m. In order to define the impulse, first define $\bar{p}$ as the spatial average of the fluid pressure on the front face of the monolithic or sandwich beams. The accumulated transmitted impulse is $I(\bar{t})=\int_0^{\bar{t}}\bar{p}(\tau)d\tau$. We have

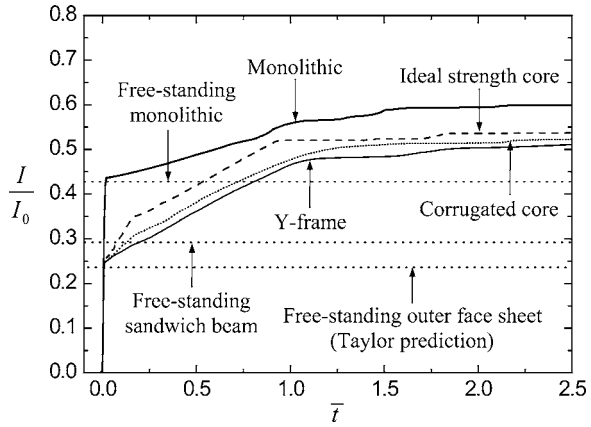

Fig. 16 Time variation of the normalized transmitted momentum I/I_o for the L=1 m clamped monolithic and sandwich beams subject to the p_o=100 MPa blast. Predictions for the final transmitted impulse in the free-standing cases are shown (for the sandwich beams an average value is given).

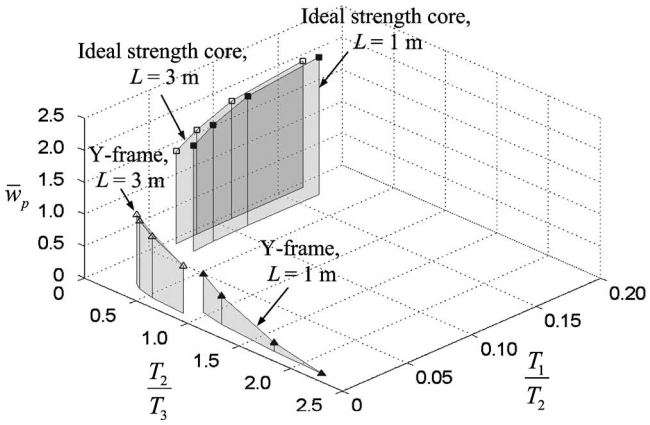

Fig. 17 A synopsis of the normalized peak deflections $\bar{w}_p$ of the Y-frame and ideal strength core sandwich beams. The axes employed are the ratios T_1/T_2 and T_2/T_3 of the durations of stages I and II and II and III, respectively, as predicted from a fully decoupled analysis. ($\bar{w}_p$ is defined as the ratio of the peak deflection as predicted from the fully coupled analysis to that predicted by a fully decoupled analysis.)

marked on Fig. 16 the final transmitted momentum as predicted by the free-standing beam analyses. Clearly, there is continued loading of the beam by the water beyond stage II, but at a much reduced pressure (for the sandwich beams, $\bar{p} \approx 0.2$ MPa for $\bar{t} > 0.25$). This pressure has a negligible effect upon the response for all beams considered, by the following argument. First, consider the sandwich beam with an ideal foam core, in which stages II and III are temporally decoupled; in the fully coupled simulations *I+II+III* of these beams, continued fluid loading is present in stage III and leads to a small additional deflection compared to the response for decoupled stage III analysis *I+II/III* (in which fluid loading is absent in stage III). This confirms that fluid loading in stage III has a negligible effect upon beam deflection. Second, consider the sandwich beams with a Y-frame or corrugated core. The beneficial coupling between stages II and III has a major effect upon the back face deflection, and the small increase in deflection due to fluid loading in stage III is masked.

7.4 Assembly of Results Into a Performance Map for Blast. Consider again the maximum midspan back face deflections of the beams with an ideal core and a Y-frame core. The dependence of these deflections upon the relative durations of the three stages of response is summarized in the three-dimensional plot of Fig. 17. The horizontal axes are T_1/T_2 and T_2/T_3[6], while the vertical axis is the ratio $\bar{w}_p$ of deflection from the fully coupled calculations *I+II+III* and from the fully decoupled calculations *I/II/III*. The predictions of $\bar{w}_p$ for the sandwich beams with a corrugated core are omitted as they lay close to the results for the beams with a Y-frame core.

The beams with an ideal foam core have high values of T_1/T_2 and a low value of T_2/T_3 due to the high transverse strength of the core. The low value of T_2/T_3 implies that the stages II and III are decoupled. The values of T_1/T_2 are sufficiently high for additional momentum transfer to occur in stage II, and thus the fully coupled calculations *I+II+III* have 50–100% larger deflections than the fully decoupled calculations *I/II/III*. This is emphasized by replotting the data in a two-dimensional graph of $\bar{w}_p$ versus T_1/T_2 in Fig. 18(*a*). It is seen that fluid loading in stage II enhances the beam deflection unless T_1/T_2 is very small (less than 0.05).

The sandwich beams with a Y-frame core lie in a different domain of the performance map (Fig. 17). The L=3 m Y-frame beams have low values of T_1/T_2 and T_2/T_3, resulting in a decoupled response from one stage to the next. Consequently, good agreement exists between the predictions of the fully coupled and fully decoupled analyses. In contrast, the L=1 m Y-frame sandwich beams display a high value of T_2/T_3, resulting in a beneficial

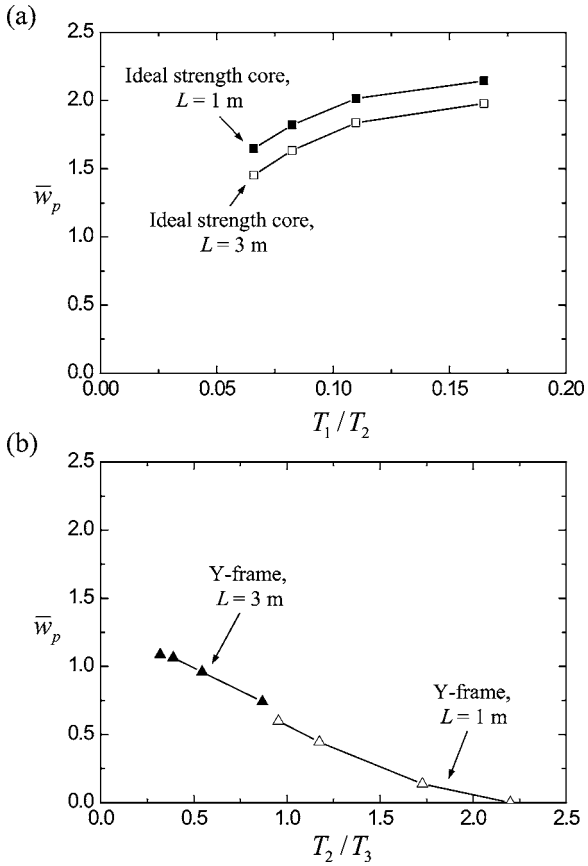

Fig. 18 The variation of $\bar{w}_p$ (*a*) with T_1/T_2 (ratio of the duration of stages I and II) for the ideal strength core beams and (*b*) with T_2/T_3 (ratio of the durations of stages II and III) for the Y-frame core beams. ($\bar{w}_p$ is defined as the ratio of the peak deflection as predicted from the fully coupled analysis to that predicted by a fully decoupled analysis.)

[6]Here the durations T_1, T_2, and T_3 are obtained from the fully decoupled analysis *I/II/III*.

coupling between stages II and III and a small deflection in the fully coupled simulations. The correlation of $\bar{w}_p$ with T_2/T_3 is summarized in Fig. 18(*b*) for the sandwich beams with a Y-frame core.

The results in Figs. 17 and 18 confirm the hypothesis presented in Sec. 2.1, viz.:

(i) the fully decoupled model underpredicts deflections when there is coupling between stages I and II (i.e., high values of T_1/T_2);
(ii) the decoupled model overpredicts deflections when coupling between stages II and III exists (i.e., high values of T_2/T_3), and
(iii) the decoupled model is adequate in the low T_1/T_2 and T_2/T_3 limit.

8 Concluding Remarks

The underwater blast response of clamped sandwich beams with a Y-frame, corrugated core and an ideal strength isotropic foam core has been investigated. The beams with a Y-frame core and corrugated core outperform the beams with an ideal foam core on the basis of rear face deflection for a beam of given mass. This is particularly true for stubby beams. All sandwich beams investigated here outperform monolithic beams of equal mass.

The Fleck and Deshpande [1] framework has been used to devise and interpret the finite element simulations. For all sandwich beams explored, the Taylor analysis based on a free-standing front face-sheet underestimates the transmitted momentum by 20–30%. This is due to continued fluid loading during the core compression phase, and leads to enhanced sandwich beam deflections.

A beneficial coupling can occur between the core compression stage and the final beam bending/stretching stage of the response for the case of stubby beams with a weak core. Consequently, cores made from a Y-frame or corrugations are superior to the stronger foam core.

The regimes of behavior of the underwater blast response of sandwich beams are usefully summarized in a performance map which takes as axes the relative duration of the three stages of response. The optimal regime is located where the initial stage of response (up to the point of first cavitation in the fluid) is decoupled from that of core compression, while the core compression phase is coupled to the beam bending/stretching phase.

Acknowledgment

The authors are grateful to ONR for their financial support through US-ONR IFO grant number N00014-03-1-0283 on "The Science and Design of Blast Resistant Sandwich Structures" and to the NIMR for support on the project "The optimal design of Y-core sandwich structures."

References

[1] Fleck, N. A., and Deshpande, V. S., 2004, "The Resistance of Clamped Sandwich Beams to Shock Loading," ASME J. Appl. Mech., **71**(3), pp. 386–401.
[2] Xue, Z., and Hutchinson, J. W., 2004, "A Comparative Study of Blast-Ressistant Metal Sandwich Plates," Int. J. Impact Eng., **30**(11), pp. 1283–1305.
[3] Taylor, G. I., 1941, "The Pressure and Impulse of Submarine Explosion Waves on Plates," *The Scientific Papers of G I Taylor* (1963), Vol. III, Cambridge University Press, Cambridge, pp. 287–303.
[4] Deshpande, V. S., and Fleck, N., 2005, "A One-dimensional Response of Sandwich Plates to Underwater Shock Loading," J. Mech. Phys. Solids, **53**(11), pp. 2347–2383.
[5] Rabczuk, T., Kim, J. Y., Samaniego, E., and Belytschko, T., 2004, "Homogenization of Sandwich Structures," Int. J. Numer. Methods Eng., **61**(7), pp. 1009–1027.
[6] Liang, Y., Spuskanyuk, A. V., Flores, S. E., Hayhurst, D. R., Hutchinson, J. W., McMeeking, R. M., and Evans, A. G., 2005, "The Response of Metallic Sandwich Panels of Water Blast," ASME J. Appl. Mech., submitted for publication.
[7] Côté, F., Deshpande, V. S., Fleck, N. A., and Evans, A. G., 2005, "The Compressive and Shear Responses of Corrugated and Diamond Lattice Materials," Int. J. Solids Struct., to appear.
[8] Côté, F., Deshpande, V. S., Fleck, N. A., and Evans, A. G., 2004, "The Out-of-Plane Compressive Behaviour of Metallic Honeycombs," Mater. Sci. Eng., A, **380**, pp. 272–280.
[9] Symmonds, P. S., 1954, "Large Plastic Deformations of Beams Under Blast Type Loading," *Proceedings of the Second US National Congress of Applied Mechanics*, University of Michigan, Ann Arbor, MI, June, pp. 505–515.
[10] Ashby, M. F., Evans, A. G., Fleck, N. A., Gibson, L. J., Hutchinson, J. W., and Wadley, H. N. G., 2000, *Metal Foams: A Design Guide*, Butterworth Heinemann, Boston.
[11] Deshpande, V. S., and Fleck, N. A., 2000, "Isotropic Constitutive Models for Metallic Foams," J. Mech. Phys. Solids **48**, pp. 1253–1283.
[12] Radford, D. D., Deshpande, V. S., and Fleck, N. A., 2005, "The Use of Metal Foam Projectiles to Simulate Shock Loading on a Structure," Int. J. Impact Eng., **31**(9), pp. 1152–1171.
[13] Sprague, M. A., 2002, "Advanced Computational Techniques for the Analysis of 3-D Fluid-Structure Interaction with Cavitation," PhD thesis, Department of Mechanical Engineering, University of Colorado.
[14] Qiu, X., Deshpande, V. S., and Fleck, N. A., 2003, "Finite Element Analysis of the Dynamic Response of Sandwich Beams Subject to Shock Loading," Eur. J. Mech. A/Solids, **22**, p. 801–814.